Kinetics and Catalysis, Vol. 44, No. 2, 2003, pp. 268–276. Translated from Kinetika i Kataliz, Vol. 44, No. 2, 2003, pp. 290–299.

Effect of Interactions between Components in Nickel–Silica Catalysts on the Yield of Carbon in Methane Decomposition

M. A. Ermakova and D. Yu. Ermakov

Boreskov Institute of Catalysis, Siberian Division, Russian Academy of Sciences, Novosibirsk, 630090 Russia

Received January 28, 2002

Abstract—A number of 90% Ni–10% SiO_2 catalysts for methane decomposition were studied at different stages of preparation and operation in the reaction using X-ray diffraction analysis, differential dissolution, temperature-programmed reduction, IR spectroscopy, and high-resolution electron microscopy. It was found that an increase in the interaction between components in the catalytic system decreased the ability of nickel to accumulate carbon in the decomposition of methane.

INTRODUCTION

Methane is the most widespread gaseous hydrocarbon and the main component of natural gas; therefore, reactions with the participation of methane are of great practical importance. Methane decomposition is one of these reactions. In the presence of catalysts (iron group metals), methane decomposes into molecular hydrogen and filamentous carbon. Hydrogen obtained in this manner is free of carbon monoxide. This is important when the presence of CO is undesirable or even inadmissible, for example, in the use of hydrogen as fuel for electrocatalytic cells, because the presence of CO results in catalyst poisoning [1, 2]. If hydrogen is not separated from methane, the mixture of these gases is a more efficient fuel for internal-combustion engines and gas-turbine power plants than natural gas or oil gas.

The second reaction product, carbon that consists of nanofibers, is of interest as a highly pure graphitized carbon material that can potentially be used in different branches of industry. Carbon fibers grow because carbon atoms, which are formed in the dissociative chemisorption of hydrocarbons on particular faces of a catalytic metal particle, diffuse to opposite faces and crystallize on them as continuous graphite-like structures [3, 4]. The rate of carbon deposition is controlled by the isothermal diffusion of carbon through a metal particle [5, 6]. Catalyst deactivation results from the blocking of the active surface by coke; however, the cause of this remains unclear.

Nickel is the most active catalyst for the decomposition of hydrocarbons, including methane. However, nickel crystallites of size greater than 100–150 nm cannot produce nanofibers; they become encrusted with carbon, which isolates them from the reaction medium. For this reason, nickel blacks and powders, which are prone to agglomeration in a hydrocarbon medium, do not produce carbon fibers and exhibit zero conversion of methane [7]. Although methane decomposition does not require high dispersity of a catalyst, promoters should be used as oxide additives that are difficult to reduce to the active component. Previously [8, 9], it was reported that carbon yields as high as 300–386 (g C)/(g Ni) were obtained with the use of nickel–silica catalysts with extremely high nickel contents in the reaction of methane decomposition; the catalysts were prepared using heterophase sol–gel synthesis. With the use of catalysts in which nickel was combined with other widespread supports such as alumina, zirconia, magnesia, and titania, the yield of carbon was much lower than that in the case of a Ni–SiO_2 sample, even though the nickel concentrations were equal and the average sizes of nickel crystallites were similar in these samples [9]. We assumed that the interaction between catalyst components (nickel–refractory oxide) affects catalytic properties in hydrocarbon decomposition reactions.

Previously, Baker and Chludzinski [10] studied the effects of various additives to Ni–Fe powders on the growth of carbon nanofibers in the decomposition of acetylene. They hypothesized that some materials (for example, Al_2O_3) can produce a physical barrier to hydrocarbon adsorption; other materials (for example, MoO_3) can decrease the solubility of carbon in the metal, but they have no effect on its diffusion; and materials of the third kind (SiO_2) can decrease both the solubility of carbon and its diffusion through a catalyst particle. However, to explain differences in the behavior of catalysts in the accumulation of filamentous carbon, it is most likely that not only the impurity material but also the preparation procedure, which is responsible for the types of interactions between components of the catalytic system, should be taken into consideration.

Thus, an understanding of the interactions between catalytic system components provides an opportunity to reasonably select an optimum catalyst for the process of methane decomposition. In this work, we continue a study of the structure and properties of previously proposed promising Ni–SiO_2 catalysts [8, 11] from the standpoint of the effect of the interaction between

0023-1584/03/4402-0268$25.00

nickel and silica on the time of catalyst deactivation in the reaction and hence on the yield of carbon in methane decomposition.

EXPERIMENTAL

Highly dispersed nickel hydroxide was prepared by hydrolysis of the ammonia complex obtained by dissolving nickel nitrate in an aqueous ammonia solution. Next, the resulting precipitate was filtered off and washed several times with distilled water to remove ammonium nitrate. After drying in air at 110°C, the specific surface area of nickel hydroxide was 460 m^2/g. Hydrated nickel oxide was prepared by the calcination of the hydroxide in a flow of air at 250°C. The specific surface area of $NiO \cdot H_2O$ was 400 m^2/g, and the coherent-scattering region was no greater than 3–4 nm in accordance with X-ray diffraction data. The texture of nickel oxide (specific surface area and pore volume) was changed by calcination for 1 h at a certain temperature within the range 350–800°C.

To prepare nickel–silica catalysts (in this case, with the composition 90%Ni–10%SiO_2), oxide precursors of nickel with different textures characteristics were impregnated with an alcoholic solution of tetraethoxysilane as a source of silica, which was prehydrolyzed in an acidic medium in the presence of a substoichiometric amount of water. The SiO_2 content of the alcosol was 0.147 g in 1 ml of solution. The hydrated nickel oxide contained 63.3 wt % Ni, which corresponded to the composition $NiO \cdot H_2O$. The other nickel oxide samples calcined at higher temperatures (350°C or higher) were stoichiometric; that is, the nickel content was ~79%. Taking into account the total pore volume of nickel oxide (6–0.7 cm^3/g depending on the calcination temperature), the hydrolyzate was diluted with ethanol so that the same amount of SiO_2 (10 wt %) was introduced in all cases. The mixture was brought to the consistency of homogeneous paste and dried in a flow of air at room temperature; thereafter, the drying temperature was increased up to 150°C.

The temperature-programmed reduction (TPR) of nickel–silica systems was performed in a U-shaped quartz tube. An argon–hydrogen mixture with a hydrogen content of 10% additionally dried with KOH was used for the reduction. The initial weight of a loaded sample was 6 mg. The flow rate of the gas mixture was 30 cm^3/min. The rate of heating was 5 K/min.

X-ray diffraction (XRD) analysis was used to determine the phase composition and dispersity of samples. The average particle sizes of nickel oxide and nickel metal were calculated from the Scherrer equation using the half-widths of (111) and (200) diffraction lines. The X-ray diffraction patterns were taken on a URD-63 diffractometer (CuK radiation, λ = 0.15418 nm) with a graphite monochromator using silicon as an internal standard.

The IR spectra were measured on a BOMEM MB-102 instrument (21 scans) with a resolution of 4 cm^{-1} at room temperature. The samples were ground with KBr in the proportion of 1.5 mg to 500 mg of KBr.

The electron-microscopic studies of the samples were performed with the use of a JEM-2010 transmission electron microscope.

The texture characteristics of the samples of nickel oxide were determined by a precision static method from the full isotherms of low-temperature (at 77 K) nitrogen adsorption with the use of an ASAP-2400 automated analyzer (Micrometrics). The calculation was performed by the BET method.

The differential dissolution method [12] was used to study the phase composition of the samples and the interactions between components. The method is based on the regularities of stoichiography and the dynamic mode of dissolution. In this method, the criterion for the separation of individual phases is the time profile of stoichiograms—the molar ratio between elements that pass into solution as a function of time. The sample weight was 3–10 mg. In the dynamic mode of dissolution, the solvent composition was varied from H_2O (pH 7) to H_2O : HCl (pH 2) or to H_2O : acid mixture (10 : 1, pH 1.2) at the component ratio H_2SO_4 : H_3PO_4 : HNO_3 : HF = 4 : 3 : 1 : 2. The process of dissolution was performed with a linear increase in the temperature at a rate of 1 K/min up to 80°C. A PST inductively coupled plasma atomic emission spectrometer was used as a detector.

The catalyst samples were tested in the reaction of methane decomposition using a laboratory setup with a vibratory fluidized-bed flow quartz reactor at a temperature of 550°C. The catalysts were prereduced in hydrogen at 550°C. Next, the reactor was cooled, and hydrogen was replaced with methane. The methane used was of 99.99% purity. The volume of the working area of the reactor was 10 cm^3. The weight of nickel in a sample was 10 mg. The flow rate of methane was adjusted to 20 cm^3/min. The concentration of hydrogen at the reactor outlet was determined by chromatography with the use of a column packed with zeolite NaX. The activity of catalysts was determined from the concentration of hydrogen in a mixture at the reactor outlet; in the case of a fresh catalyst, this value was 28–30%. The reaction was stopped when the concentration of hydrogen decreased to 5%. The conversion of methane was determined using the equation

$$X = \frac{1 - c}{1 + c} \times 100\%,$$

where c is the methane concentration in volume (mole) fractions at the reactor outlet.

The amount of carbon deposited on the catalyst during the reaction time was determined by weighing the unloaded samples. The yield of carbon (G, (g C)/(g Ni)) was calculated as follows: the amount of deposited car-

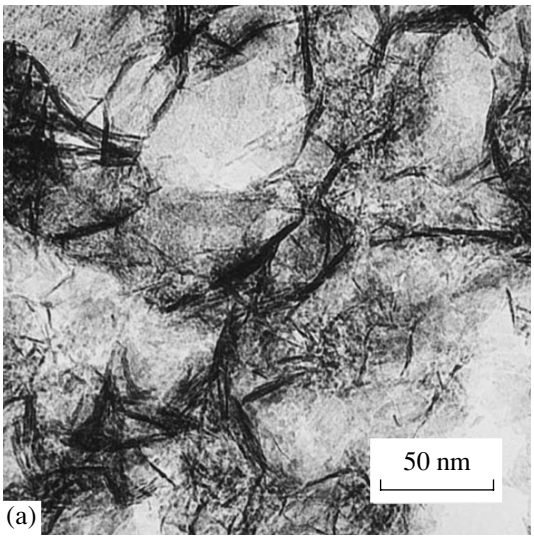

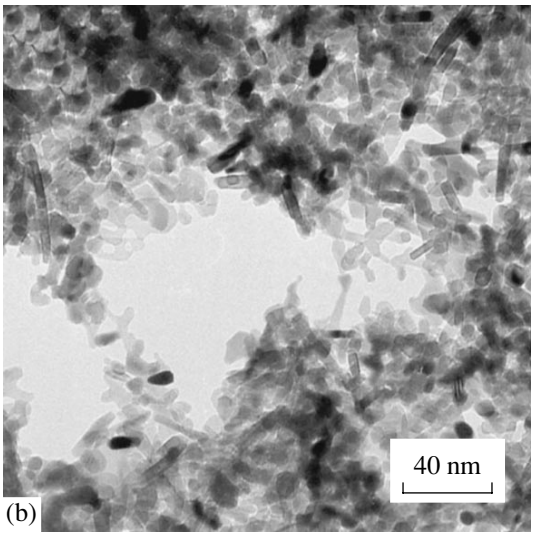

Fig. 1. Electron micrographs of nickel oxides prepared by the calcination of α-$Ni(OH)_2$ at (a) 250 and (b) 400°C.

bon was divided by 0.01 g, where 0.01 g is the weight of nickel in the catalyst sample.

RESULTS AND DISCUSSION

Figure 1a demonstrates the micrograph of highly dispersed hydrated nickel oxide prepared by the calcination of the hydroxide at 250°C. The formation of a weakly crystallized oxide phase at this temperature was supported by X-ray diffraction analysis, and this is consistent with published data [13]. Judging from the structure, this oxide is a pseudomorphosis on the initial substance, α-nickel hydroxide. The hydrated oxide was divided into six portions. One of them remained unchanged, and the other five portions were calcined for 1 h at different temperatures. Table 1 summarizes the texture characteristics of nickel oxide samples depending on the calcination temperature. Starting with 350°C, the finest flat flakes of the parent oxide were agglomerated to form bulk particles with a face-centered cubic lattice and an average size of 8 nm, whereas the average size of nickel crystallites increased up to 12 nm at 400°C (Fig. 1b). As the calcination temperature was further increased, the particle size of nickel oxide further increased because of coalescence (Table 1).

Table 2 summarizes the characteristics of a number of 90%Ni–10%SiO_2 catalysts, which were prepared by treating the corresponding NiO samples with an alcosol and were reduced with hydrogen at 550°C. It can be seen that the yield of carbon strongly depends on the dispersity of nickel oxide used as the catalyst precursor rather than on the average size of nickel particles in the reduced samples. Thus, at almost the same average particle size of nickel in catalysts 1 and 2, the yield of carbon on sample 2 was many times higher. This considerable increase in the yield of carbon is difficult to explain by the small increase in the average size of metal particles. Indeed, the average size of nickel particles in samples 2–5 increased from 10 to 60 nm, whereas the yield of carbon increased by only 22%. Because the nickel content of all the catalyst samples was the same (90 wt %), the difference in the yields of carbon can be explained only by taking into account the presence or absence of unreduced silicates in the catalyst. These silicates can be formed at the stage of mixing nickel oxide with the hydrolyzate. In the test series, the oxide precursor of sample 1 exhibited a maximum surface area of 400 m^2/g; it was hydrated and hence most reactive in terms of the formation of silicate compounds through its interaction with polysiloxane molecules from the alcosol. At a calcination temperature of 350°C or higher, the particles of nickel oxide coarsened; in this case, the amount of hydroxyl groups at their surface dramatically decreased; as a consequence, the reactivity of the surface decreased. Evidently, a tendency to form silicate compounds upon treatment with the alcosol is much weaker in the case of nickel oxide samples 2–5 than that in sample 1.

To test this hypothesis, samples 1 and 5 (henceforth, the sample numbers are given in accordance with Table 2) were studied in detail at different stages of preparation and in the reaction of methane decomposition, because these samples are characterized by extreme yields of carbon in the test series of catalysts (40 and 384 (g C)/(g Ni), respectively). At the same nickel content, the time it takes for the complete deactivation of these catalysts in the reaction differed by a factor of ~10; this difference also resulted in different yields of carbon (Fig. 2). Note that the curves of methane conversion for catalysts 2–4 are similar to the curve obtained with catalyst 5 and almost coincide with it. Differences were observed only in the last 400–500 min of the reaction.

Nickel oxides with surface areas of 400 and 7 m^2/g, which were prepared by calcination at 250 and 700°C, respectively, were used as the precursors of samples 1

Table 1. Texture and structure characteristics of NiO samples depending on calcination temperature

Sample	Calcination temperature, °C	S_{sp}, m^2/g	Volume of 1- to 100-nm pores, cm^3/g	Volume of micropores, cm^3/g	Average pore size, nm	Average particle size of NiO, nm (XRD)
1	250	400	1.09	0.0246	17	3–4
2	350	144	0.57	0.0102	18	8
3	400	90	0.40	0.0013	20	12
4	450	56	0.28	0.0002	19	19
5	700	7	0.03	–	21	~90
6	800	3	0.013	–	20	>100

Table 2. Average size of nickel particles in reduced catalysts (90% Ni–10% SiO_2) and the yields of carbon on them

Sample	Average particle size of NiO*, nm (XRD)	Average particle size of NiO, nm		Yield of carbon, (g C)/(g Ni)
		(XRD)	(EM)	
1	3–4	7	6.8	40
2	8	10	9	300
3	12	12	12	375
4	19	17	16	375
5	~90	60	62	384
6	>100	>100	–	2

Note: * For samples used as catalyst precursors before the treatment with tetraethoxysilane.

and 5, respectively. Figure 3 demonstrates the TPR profiles of catalysts 1 and 5. The TPR profiles of parent oxides are given for comparison. It can be seen that two peaks of hydrogen absorption with maximums at 236 and 246°C were observed in the reduction of highly dispersed silica-free nickel oxide. Note that the former peak was observed only in the reduction of NiO that was prepared at temperatures lower than 400°C. According to Mile *et al.* [14], this effect is associated with the conversion of "Ni_2O_3" to NiO. The presence of nonstoichiometric nickel oxide species in nickel(II) oxide was also mentioned by other researchers [15]. The conversion of Ni^{2+} into Ni^0 began at 240°C and occurred over a very narrow range of temperatures to complete at 255°C. In this case, even though the reduction temperature was low, the average size of nickel crystallites (according to XRD data) increased as compared to that of the parent oxide particles (3–4 nm) by an order of magnitude and was as large as 44 nm.

An analysis of the TPR profile obtained by the reduction of sample 1 (Fig. 3) indicated that the addition of silica to nickel oxide significantly increased the temperature of sample reduction and broadened the second peak of hydrogen absorption. In this case, according to XRD data, the average size of nickel crystallites decreased to 7 nm. This was also supported by electron-microscopic data (Fig. 4a).

The oxide precursor of sample 5 (NiO with S_{sp} = 7 m^2/g) was reduced starting at a temperature of 300°C. The rate of hydrogen absorption reached a maximum at 332°C, and the reduction was complete at 380°C (Fig. 3). This reduction behavior is characteristic of stoichiometric nickel oxide [16]. After the modification of this oxide with silica, the reduction started at the specified temperature and stopped at 450°C, which is higher than the reduction temperature of unmodified nickel oxide by 70°C. The peak was split into two new peaks with maximums at 335 and 370°C. It is likely that the first maximum can be ascribed to NiO unbound to silica, whereas the second peak characterizes the reduction of bound oxide species. In contrast to sample 1, the peak that characterizes the reduction of sample 5 exhib-

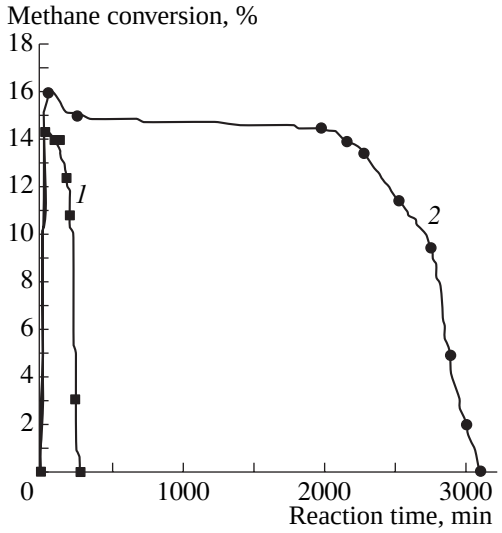

Fig. 2. Methane conversion at 550°C on catalysts (*1*) 1 and (*2*) 5 as a function of reaction time.

ited no tailing; this fact indicates that the interaction between components in the test system was weak. Figure 4b demonstrates the micrograph of reduced sample 5. It can be seen that, in contrast to sample 1 (Fig. 4a), sample 5 consisted of coarse nickel particles. The system was fairly uniform, although relatively small nickel crystallites were present (<25 nm). A translucent silica film, which prevents particles from agglomeration, can be seen at the edges of metal particles.

We used IR spectroscopy to reveal differences in the interaction of phases in samples 1 and 5 at different stages of preparation. We compared the IR spectra of samples (Fig. 5) only within a frequency region from 200 to 1300 cm^{-1}, because changes in the absorption profile characterizing nickel–silica interactions were observed in this region. At frequencies higher than 1300 cm^{-1}, all the IR spectra of the test samples exhibited absorption bands due to impurity anions (at 1305 and 1380 cm^{-1}) and absorption bands that correspond to deformation (at 1630 cm^{-1}) and stretching vibrations of water (a broad absorption band with a maximum at 3440 cm^{-1}).

It can be seen in Fig. 5 that bands with maximums at 583 (≡Si–OH deformation vibrations), 950 (≡Si–OH stretching vibrations), and 793 cm^{-1} (symmetric ≡Si–O–Si≡ stretching vibrations, which are typical of a silica skeleton) disappeared from the spectrum of sample 1, whereas these bands were present in the IR spectrum of the pure xerogel (the alcosol was dried and calcined at 150°C) [17]. All these data, as well as the strong shift of the most intense absorption band of silica at 1078 cm^{-1} (asymmetric ≡Si–O–Si≡ stretching vibrations of the skeleton) toward lower frequencies (to 1050 cm^{-1}), are indicative of the presence of the ≡Si–O–Ni≡ bond. As noted previously [18, 19], the most intense band of

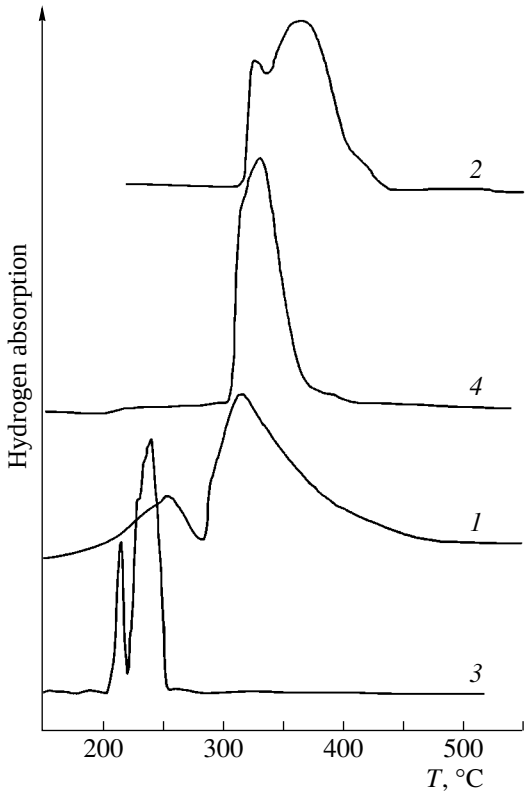

Fig. 3. TPR profiles obtained in the reduction of catalysts (*1*) 1 (NiO (250°C) + 10% SiO_2) and (*2*) 5 (NiO (700°C) + 10% SiO_2) and the corresponding parent nickel oxides (*3*) NiO (250°C) and (*4*) NiO (700°C) (oxide calcination temperatures are given in parentheses); the heating rate was 5 K/min; the sample weight was 6 mg; and the flow rate of the gas mixture was 30 cm^3/min.

silica is sensitive to the formation of silicate compounds. A comparison with the samples of SiO_2 and NiO (250°C) indicates that the bands at 450 and 630 cm^{-1} in the spectrum of sample 1 remained unchanged and belonged to the deformation vibrations of the silica skeleton and the O–H group in hydrated nickel oxide, respectively. Thus, we can state that silica introduced into a porous matrix of hydrated nickel oxide is chemically bound with the formation of silicate compounds because of the high surface area (400 m^2/g) and the specific layered structure of the hydrated nickel oxide. Dzis'ko *et al.* [20] related the appearance of bands at 665 and 1050 cm^{-1} in consecutively precipitated and coprecipitated nickel–silica samples to strong chemical interactions and the formation of a new chemical compound. The shift of a band at 1100 cm^{-1} to 1050 cm^{-1} was attributed in [21, 22] to the formation of poorly crystallized 1 : 1 phyllosilicate of the nepouite type ($Ni_3Si_2O_5(OH)_4$).

An analysis of the IR spectrum of compound 1 after reduction indicated that silicate compounds formed on mixing the components (nickel oxide and the alcosol) did not disappear, although the reduction temperature

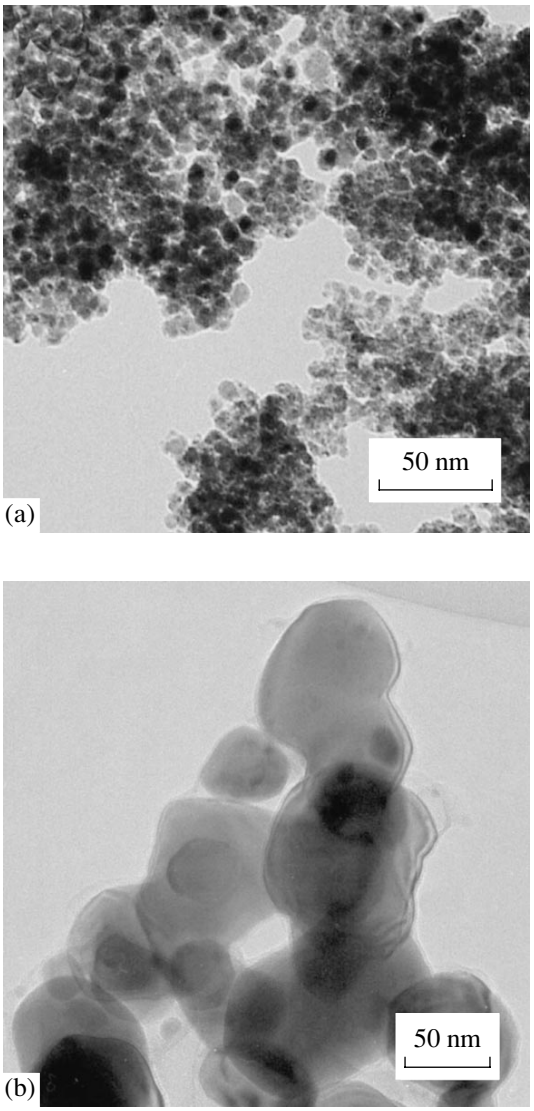

Fig. 4. Electron micrographs of catalysts after reduction in H_2 at 550°C: (a) catalyst 1 and (b) catalyst 5.

was high (550°C). As judged from the shift of the main band of silica to 1030 cm^{-1}, as well as from the appearance of a weak band at 670 cm^{-1}, we can conclude that instable silicate compounds of the nepouite type were converted into more stable talcite-like compounds [22].

Let us analyze in the same manner the IR spectra of sample 5 at different stages of preparation. The IR spectrum of this sample (oxide form) seems to be a superposition of the spectra of SiO_2 (150°C) and NiO (700°C). In this spectrum, adsorption bands at 455 and 460 cm^{-1}, which are characteristic of the deformation vibrations of SiO_2 and the stretching vibrations of NiO, respectively, are superimposed on each other to merge into a single more intense band. In the oxide sample of catalyst 5, a band at 1078 cm^{-1}, which corresponds to the asymmetric stretching vibrations of SiO_2, was somewhat shifted to the low-frequency region (to 1070 cm^{-1}); this

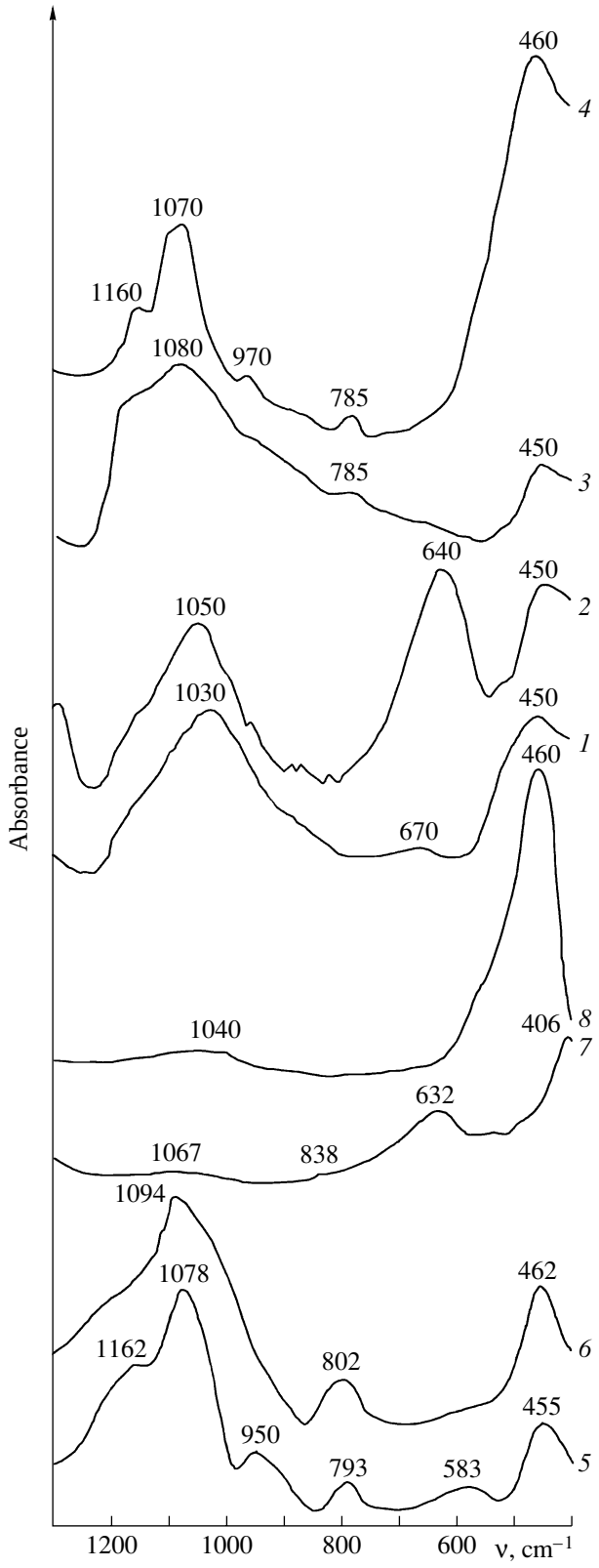

Fig. 5. IR spectra of catalysts (*1*, *2*) 1 and (*3*, *4*) 5 (*2*, *4*) before reduction and (*1*, *3*) after reduction in H_2 at 550°C; SiO_2 samples heated at (*5*) 150 and (*6*) 600°C; and NiO samples used for the preparation of catalysts and calcined at (*7*) 250 and (*8*) 700°C.

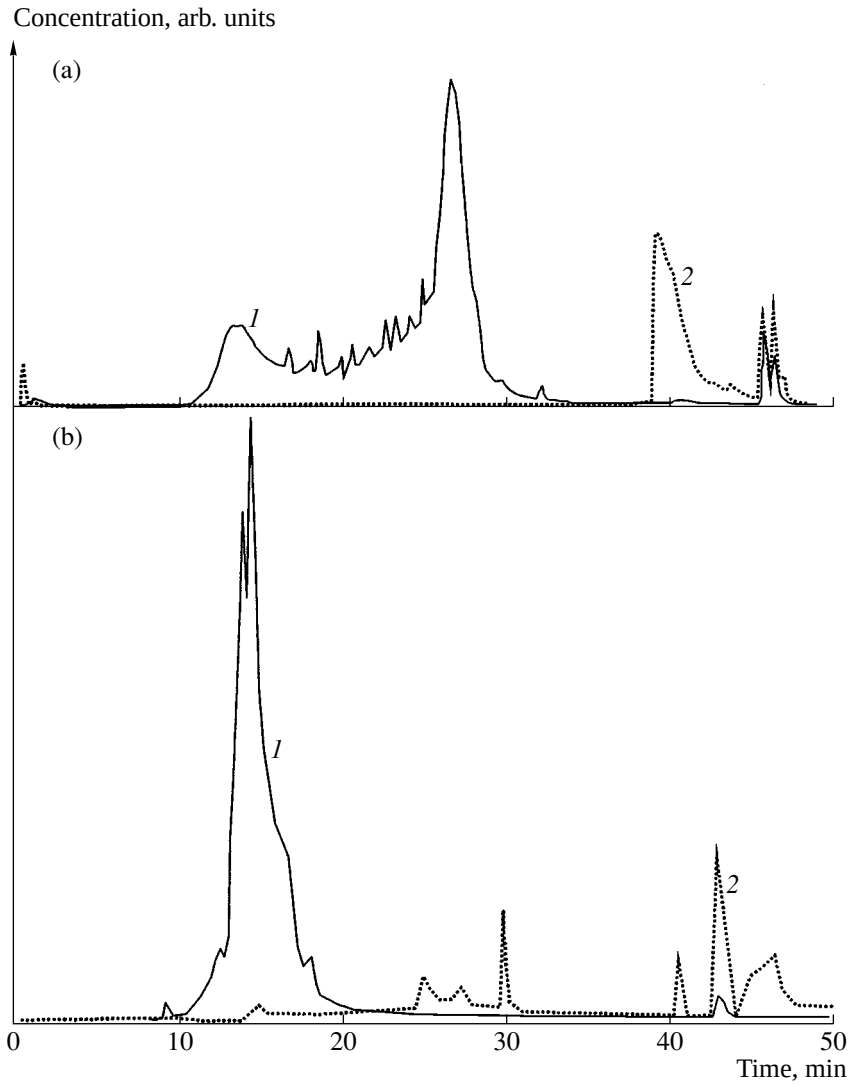

Fig. 6. Differential dissolution profiles of reduced samples (a) 1 and (b) 5: (*1*) nickel and (*2*) silica.

suggests the appearance of weak interactions at the NiO–polysiloxane film interface. Upon the reduction of sample 5 at 550°C, its IR spectrum became similar to the spectrum of SiO_2 (600°C); this fact is indicative of a minimum interaction between the components of the binary system under consideration.

Figure 6 demonstrates the differential dissolution profiles of reduced samples 1 and 5. This method supported the presence of silicate compounds in sample 1. The dissolution curves of nickel and silica exhibited synchronous peaks after approximately 45 min; these peaks are indicative of the dissolution of a chemical compound, which can be characterized as nepouite because the Ni/Si ratio is 1.5 and corresponds to the stoichiometry of nepouite. The concentration of nepouite was no higher than 2% of the reduced sample weight. As for sample 5, the dissolution curve of nickel also exhibited a small peak after 40 min; the maximum of this peak coincides with the maximum of a much more intense peak of silica dissolution. This fact indicates that a very small portion of nickel in sample 5 can also be chemically bound to silica; however, in this case, it is difficult to speak of stoichiometry. Because the difference in the peak intensities is very great, we can only state that the amount of bound nickel in sample 5 is much lower than that in sample 1.

The behavior of catalysts for methane decomposition over the first minutes after being placed in a reaction medium is of paramount importance because it is responsible for the course of the subsequent reaction over many hours. Figures 7a and 7c demonstrate the micrographs of catalysts 1 and 5, respectively, after the first 30 min of reaction. It is well known that, when a catalyst is placed in methane, free metal particles acquire an increased fluidity under the action of dissolved carbon, and they can coalesce to very large sizes, even though a support is present in the catalyst [23]. This explains why initially disperse catalyst 1 (the aver-

age particle size of Ni d_{Ni} is ~7 nm) produced both thin and thick carbon fibers with nickel crystallites as great as 120 nm in size at the ends of the fibers (Fig. 7a). The uncoalesced small particles can be subdivided into those at which fibers grew and those covered with carbon; the latter are much greater in number. It is evident that this behavior of the catalyst is a consequence of the strong interaction of nickel with silica, as supported by TPR, IR spectroscopy, and differential dissolution. Nickel silicates that remained unreduced decreased the rate of carbon diffusion through nickel nanoparticles; because of this, they became covered with carbon formed in methane decomposition and deactivated. Because these particles constitute the major portion of catalyst 1, it is most likely that this is responsible for a low yield of carbon on this catalyst.

In contrast to catalyst 1, catalyst 5 produced carbon fibers of approximately equal diameters within a range of 80–118 nm (Fig. 7c), which is much the same as the particle size of Ni in the reduced catalyst (Fig. 4b). The nickel particles at the ends of fibers are well-faceted crystals, which acquired this shape under exposure to a reaction medium [24]. Nickel particles encapsulated in carbon are absent from the micrograph. Thus, the behaviors of catalysts 1 and 5 over the first hour of reaction supported the conclusion that the strong interaction between nickel and silica has an extremely adverse effect on the yield of carbon.

Data for sample 6 are also given in Table 2. The yield of carbon on this catalyst was no higher than 2 (g C)/(g Ni), although it is evident that the interaction between components in this sample was even weaker than that in sample 5. However, this fact can be easily explained. Nickel oxide used for the preparation of catalyst 6 was calcined at 800°C, and its surface area was no higher than 3 m^2/g. Based on this surface area, the average size of oxide particles was equal to 270–300 nm. The stabilization of this coarsely dispersed oxide system by the addition of silica did not allow us to prepare a catalyst with optimum structure characteristics because the size of nickel crystallites did not decrease after reduction (dispersion did not occur); consequently, this size was greater than the critical size (150–200 nm) for the production of fibers.

Thus, we found that the interaction between components of the catalytic system depends on the specific surface area of nickel oxide used as a precursor. The most disperse nickel oxide with a specific surface area of 400 m^2/g exhibited the greatest tendency to form silicates on treatment with a solution of hydrolyzed tetraethoxysilane followed by reduction. The calcination of this oxide at higher temperatures (350–700°C) decreased the reactivity of its surface toward silica and hence facilitated a decrease in the amount of residual silicates in the reduced catalyst.

The yield of carbon depends on the interaction between nickel and silica. The presence of ~2% silicates decreased the yield of carbon down to 40 (g C)/(g Ni).

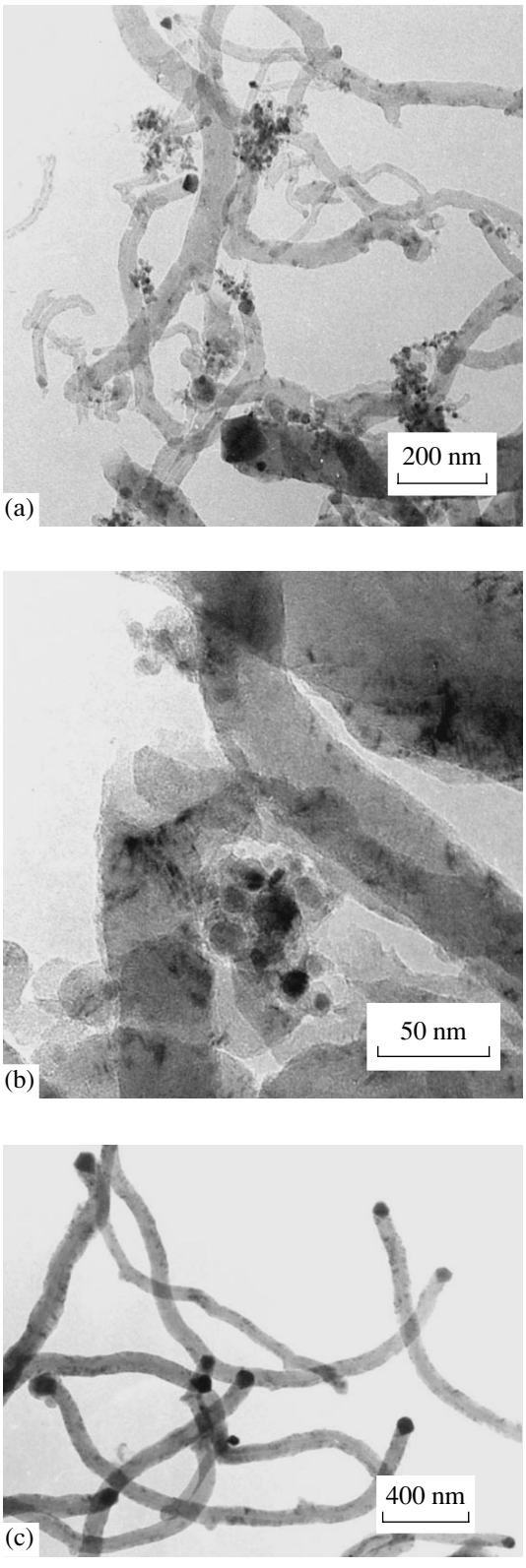

Fig. 7. Electron micrographs of catalysts after exposure to methane for 30 min: (a) carbonized catalyst 1, (b) finest particles of catalyst 1 encapsulated in carbon, and (c) carbonized catalyst 5.

The catalyst in which silicates were not detected after reduction was characterized by a carbon yield of 384 (g C)/(g Ni).

ACKNOWLEDGMENTS

We are grateful to Cand. Sci. (Chem.) A.L. Chuvilin for the provision of micrographs, to Cand. Sci. (Chem.) G.N. Kustov for the measurement of IR spectra, and to Dr. Sci. (Chem.) V.V. Malakhov and L.S. Dovlitova for the provision of data on the differentiated dissolution of samples.

REFERENCES

1. Kuvshinov, G.G., Mogilnykh, Yu.I., Kuvshinov, D.G., Parmon, V.N., and Zavarukhin, S.G., *Proc. 11th World Hydrogen Energy Conference*, Stuttgart, 1996, p. 2.
2. Zhang, T. and Amiridis, M.D., *Appl. Catal., A*, 1998, vol. 167, p. 161.
3. Baker, R.T.K., Barber, M.A., Harris, P.S., Feates, F.S., and Waite, R.J., *J. Catal.*, 1972, vol. 26, p. 51.
4. Fenelonov, B., Likholobov, V.A., Derevyankin, A.Yu., and Mel'gunov, M.S., *Catal. Today*, 1998, vol. 42, p. 341.
5. Rodriguez, N.M., *J. Mater. Res.*, 1993, vol. 8, p. 3233.
6. Holstein, W.L., *J. Catal.*, 1995, vol. 152, p. 42.
7. Kim, M.S., Rodriguez, N.M., and Baker, R.T.K., *J. Catal*., 1991, vol. 131, p. 60.
8. Ermakova, M.A., Ermakov, D.Yu., Kuvshinov, G.G., and Plyasova, L.M., *J. Catal.*, 1999, vol. 187, p. 77.
9. Ermakova, M.A., Ermakov, D.Yu., Kuvshinov, G.G., and Plyasova, L.M., *Kinet. Katal.*, 1998, vol. 39, no. 5, p. 791.
10. Baker, R.T.K. and Chludzinski, J.J., *J. Catal.*, 1980, vol. 64, p. 464.
11. Ermakova, M.A., Ermakov, D.Yu., and Kuvshinov, G.G., *Appl. Catal., A*, 2000, vol. 201, p. 61.
12. Malakhov, V.V. and Vlasov, A.A., *Kinet. Katal.*, 1995, vol. 36, no. 4, p. 503.
13. Bihan, S.Le. and Figlarz, M., *Thermochim. Acta*, 1973, vol. 6, p. 319.
14. Mile, B., Stirling, D., Zammit, M.A., Lovell, A., and Webb, M., *J. Catal.*, 1988, vol. 114, p. 217.
15. *Chemistry of the Solid State*, Garner, W.E., Ed., London: University of Bristol, 1955.
16. Robertson, S.D., McNicol, B.D., De Baas, J.H., Kloet, S.C., and Jenkins, J.W., *J. Catal.*, 1975, vol. 37, p. 424.
17. Ro, J. and Chung, I.J., *J. Non-Cryst. Solids*, 1991, vol. 130, p. 8.
18. Lazarev, A.N., *Kolebatel'nye spektry i stroenie silikatov* (Vibrational Spectra and the Structyure of Silicates), Leningrad: Nauka, 1968.
19. Sviderskii, V.A., Voronkov, M.G., Klimenko, V.S., and Klimenko, S.V., *Zh. Prikl. Khim.*, 1997, vol. 70, p. 1698.
20. Dzis'ko, V.A., Noskova S.P., Karakchiev L.G., Borisova M.S., Bolgova V.D., and Tyulikova T.Ya., *Kinet. Katal.*, 1972, vol. 13, no. 2, p. 366.
21. Clause, O., Kermarec, M., Bonneviot, L., Villain, F., and Che, M., *J. Am. Chem. Soc.*, 1992, vol. 114, p. 4709.
22. Kermarec, M., Carriat, J.Y., Burattin, P., Che, M., and Decarreau, A., *J. Phys. Chem.*, 1994, vol. 98, p. 12008.
23. Ermakova, M.A., Ermakov, D.Yu., Plyasova, L.M., and Kuvshinov, G.G., *Catal. Lett.*, 1999, vol. 62, p. 93.
24. Chesnokov, V.V. and Buyanov, R.A., *Rus. Chem. Rev.*, vol. 69, p. 623.